CONCEPT FOR A HYDROGEN-POWERED AIRCRAFT FOR 150 PASSENGERS WITH EIS 2035

J. Stürken*, L. Meinberg*, S. Bahm*, M. Seibt*, S. Kotlarov*, T. Welsch*, T. Effing†, E. Stumpf‡
* Graduate student
† Research associate and PhD student
‡ Head of institute
Institute of Aerospace Systems, RWTH Aachen University, Wüllnerstraße 7, 52062 Aachen, Germany

Abstract

In this work, a short/medium-haul aircraft for 150 passengers is presented. It is powered exclusively by hydrogen to minimize the environmental impact while optimizing the aircraft's performance at the same time. The concept, named HyZero, was developed as part of the NASA/DLR Design Challenge 2021. The basis for the development of HyZero is the identification of specific aircraft requirements and a methodical comparison of different configurations. The design is not only driven by typical key parameters, such as aerodynamics or weight, but also by the best possible integration of a cryogenic liquid hydrogen tank. The aircraft's concept includes the structural design, mission analysis, and a description of the required airport and hydrogen infrastructure. HyZero is compared with a reference aircraft, which is powered with a blend of 30% Sustainable Aviation Fuel. To assess HyZero's climate impact, CO_2-equivalent emissions and fuel consumption are calculated and an optimum between fuel consumption and climate impact is determined. The direct operation costs (DOC) of HyZero are determined using the CeRAS method for an average flight mission. Finally, the costs and the environmental impact considering the emission of greenhouse gases are compared between HyZero and the reference aircraft. The most important design features include a hybrid drive train, a lifting body, and high aspect ratio strut-braced wings. The result is that while HyZero reduces the CO2-equivalent emissions by a factor of 33 the DOC are 95% higher than those of the reference aircraft. This shows that further work is required to make such an aircraft not just environmentally, but also economically feasible.

Keywords
Hydrogen; Climate Impact; Design Concept

1. INTRODUCTION & APPROACH

In 2019, the European Union (EU) presented the European Green Deal, which sets the goal of achieving climate-neutrality by 2050. Aviation is currently responsible for 3 % of global CO_2-emissions and the aviation industry has intensified its efforts to develop and implement climate-neutral flying [1]. Innovative and sustainable approaches will be required to meet the enormous economic and ecological challenges in the coming years. To achieve the goals of the Green Deal, the use of hydrogen as a primary energy source in aviation holds great potential [2]. However, there is currently no aircraft ready for serial production that runs entirely on hydrogen. The HyZero concept was developed in the context of the NASA/DLR Aeronautical Design Challenge 2021, which recognises the need for innovation in clean aviation by calling for the design of a hydrogen-powered, short- to medium-haul aircraft with a maximum passenger capacity of 150 passengers (PAX) and an entry into service (EIS) in 2035. An additional Top Level Aircraft Requirement (TLAR) is the ability to fulfill two reference missions of 600 km and 2 000 km, respectively.

The design is compared with a reference aircraft at a 2035 technology level, which is based on the 150-PAX CeRAS CSR-01 dataset commonly used in conceptual aircraft studies [3]. To develop a reference aircraft in line with HyZero's targeted market entry, the CSR-01 is fitted with the CFM International LEAP-1A35A engines used on the Airbus A319neo, with their performance extrapolated to 2035. In addition, a carbon-fibre-reinforced-polymer (CFRP) fuselage is added. The reference aircraft is fueled by kerosene with 30 % Sustainable Aviation Fuel (SAF) added. Its mission profile is changed from that of HyZero to be more optimized for a conventionally-fueled aircraft. This allows for a meaningful comparison between the two aircraft.

Based on a methodical idea generation and selection process, an aircraft concept is developed that is tailored to future, environmentally-friendly air transport. Cost and operational assessments are made focussing on the German and European aviation market; how-

doi: 10.25967/550400

ever, the concept is generally applicable to international markets
This work is structured as follows:

- In Section 2, the derived concept is introduced and explained in detail.
- The technical data, namely mass estimation and aerodynamic data, is listed in Section 3.
- In Section 4, the necessary changes to airport and hydrogen infrastructure are discussed.
- Results of the mission analysis, containing Flight Path Optimization, Climate Impact, Fuel Consumption, and DOC Analysis, are presented in Section 5.
- Section 6 concludes the results.

2. CONFIGURATION

To identify the optimal aircraft configuration, a wide variety of concepts from literature are evaluated and narrowed down to the final HyZero design. HyZero is a fixed-wing aircraft with a V-tail (cf. Figure 1). The high wing has a high aspect ratio and is supported by struts. The tank, which contains two independent compartments separated by a dividing wall, is located in the rear of the aircraft. Instead of an elliptical shape, the fuselage cross-section features a double-D profile. The two main engines are mounted under the wing. In addition, a boundary layer ingesting (BLI) fan, powered by a fuel cell, is integrated at the rear of the fuselage. The main aircraft dimensions and characteristics are gathered in Table 1 Figure 1 also contains the geometric proof for the clearance angles. The calculation of the remaining values from Figure 1, as well as the design process as a whole, are discussed in the following sections.

Table 1. HyZero data

Length	35.82 m
Height	8.06 m
MTOM	59 132 kg
Wing area	119 m^2
Aspect ratio	19.55
Anhedral	3°
Sweep leading edge	9.16°
Taper ratio	0.5
Empennage area	36.37 m^2
Take-off field length dry	1 553.5 m
Landing field length	980.3 m
Climb rate	1 700 ft/min
Cruise speed	Ma 0.7
Cruise altitude	FL 290
Glide ratio	18.86

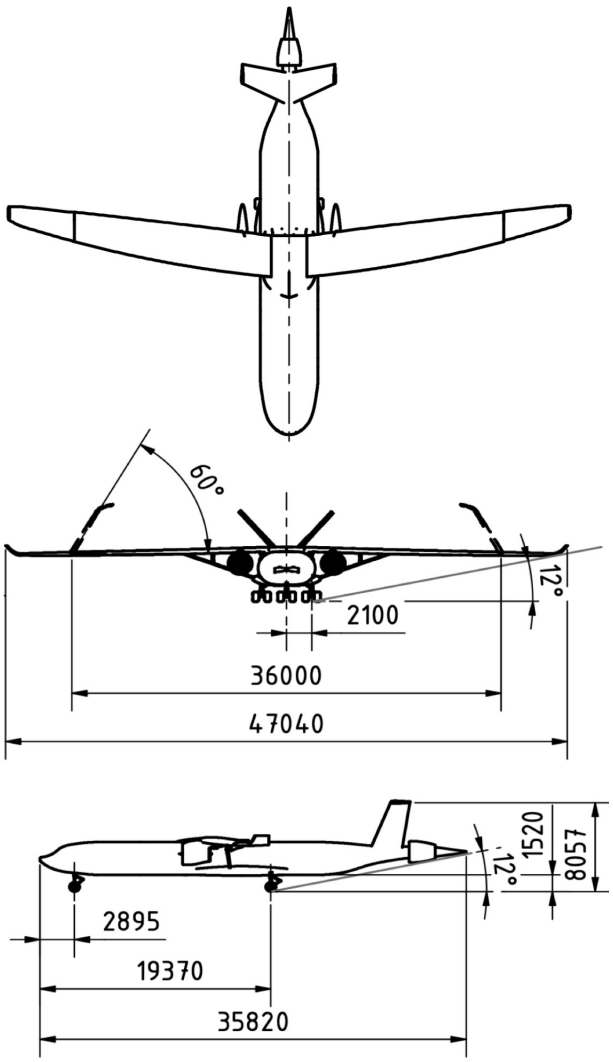

Figure 1. General Arrangement

2.1. Fuel and Tank

For powering HyZero by using hydrogen, the storage condition and method on board is discribed in the following.

2.1.1. Fuel Selection

One possible classification of hydrogen storage technologies is the segmentation into physical storage, adsorption, and chemical storage. Adsorption and chemical storage are largely differentiated by the carrier material. Because of the necessity to use these carrier materials, adsorption and chemical storage methods suffer from either low volumetric or gravimetric energy densities, and are deemed unsuitable for aircraft applications in 2035 [4]. Physical storage includes compressed, liquified, and cryo-compressed hydrogen. Table 2 summarizes key characteristics of these methods and allows for a rough comparison, although values vary between tank sizes and applications [5–7].
In addition to safety, mass and volume are the two most important characteristics of a hydrogen tank system for aircraft applications. Liquid hydrogen (LH_2) systems exhibit the highest gravimetric system densi-

Table 2. Gravimetric density of physical hydrogen storage methods [5–7]

	Grav. density [wt %]
Compressed, 700 bar	5.2
Compressed, 350 bar	5.5
Cryo-compressed, 300 bar	5.4
Liquid at 20 K, 1 bar	7.5

ties. This stems from the high mass of the pressure vessels required for compressed and cryo-compressed storage. In addition, pressure vessels are costly and limited to near spherical or cylindrical shapes [5]. Under consideration of other factors such as transportability and handling of hydrogen, and the energy requirement for compression and liquification, LH_2 is selected as the fuel for HyZero.

2.1.2. Tank Placement

To minimize heat influx and boil-off, the surface of the LH_2 tanks must be minimized, leading to compact, near-spherical or cylindrical shapes. This makes tank integration into HyZero's wings unfeasible. Since the tanks must be placed outside of the pressurized cabin for safety reasons [8], and cargo space cannot be reduced, the only options seen as reasonable are in front or behind the cabin, or under the wing as removable tanks. Because of the decision to place the BLI fan at HyZero's aft section, placing the tanks in the front section of the fuselage is dismissed due to the prohibitively long fuel lines this would require. Removable tanks under the wing offer the benefit of allowing not only the reduction of fuel mass, but also fuel tank mass for the shorter, 600 km mission. They also have the potential to significantly simplify the refueling process. External tanks are widely used by military fighter aircraft and have been proposed by Airbus for their future hydrogen aircraft, albeit as standalone propulsion units [9]. The additional drag from external pods for an Airbus A321 was evaluated by Dangi and Patel [10]. Even for the most favourable option, total drag force still increased by 26.51 % [10]. In the same study, an increase in length of the aircraft to accommodate the hydrogen tanks increases drag by only 6.85 % [10]. For this reason, the option of using external tanks is dismissed.
This leaves the space behind the cabin as the only feasible option. A benefit of the fuel placement within the fuselage, as opposed to the wing, lies in the fact that their aerodynamic shape can be optimized and innovative concepts such as morphing wings, which are discussed in section 2.3, can be implemented.

2.1.3. Tank Design

The single tank with two compartments is designed as an integral, load-carrying part of the fuselage, as this leads to reductions in structural mass [11]. The tank is insulated externally, as there is currently no material available, or likely to be available until 2035, that can sufficiently prevent permeation through the insulation [12].
Composite tank walls can provide a 25 % weight saving over aluminium tanks [13]. Despite their higher cost, a composite tank design is adopted to keep the center of gravity within an acceptable range. A liner made of aluminium is necessary to prevent the hydrogen from leaking through the composite material [11]. Verstraete et al. [14] explore multi-layer insulation (MLI) and foam insulation for applications comparable to those of HyZero. While MLI provides a weight advantage over foam for the same level of heat flux, its use of a high vacuum makes it more expensive to install and maintain, and carries the risk of catastrophic failure in case the vacuum is lost [14]. In addition, the use of foam insulation only requires a single structural tank wall rather than two. The outer tank wall only serves as a barrier between the foam and the environment [11]. A polyurethane foam is selected as it achieves the lowest mass [14].
The tank is integrated into the fuselage according to the description by Brewer [11]. Thus, it features a dividing wall that creates two separate and therefore redundant compartments, which ensures that the main engines can be fed from separate tanks during takeoff. Additional dividers reduce sloshing [11]. The inner, structural tank wall thickness is calculated using the pressure vessel equation, which additionally considers a safety factor [15]. It also depends on the tank diameter, resulting in a varying wall thickness. The outer tank wall features a constant thickness as it constitutes the aircraft fuselage. The separating wall in the middle is calculated similarly to maintain redundancy in case one compartment leaks. Using a density of $1\,800\,\mathrm{kg/m^3}$, the resulting tank mass amounts to 1 090 kg.

2.2. Fuselage

HyZero's fuselage combines a lifting shape with a windowless design, which are described in this section.

2.2.1. Lifting Fuselage Design

HyZero's fuselage is a lifting body with a Double-D cross-section modelled on the Aurora D8 concept [16]. The technology is expected to be available for commercial applications in 2035 [17]. Due to the non-circular shape of the cabin, the internal cabin pressure leads to significant bending stresses at the transition of the circumference of half-cylinders to the straight upper and lower sections, which can be absorbed by vertical partitions of the cabin. Based on the PRSEUS model [18], the fuselage is made of carbon fibre preforms [19, 20]. Despite these complications, the lifting body design offers significant advantages over the conventional design. Since the tank plays the most important role in the HyZero design, the fuselage is optimized around the tank. The fuselage width of 4.48 m and its height of 2.98 m allow for 2-4-2 double-aisle seating, which is unusual in the short-haul aircraft class. The overall

length of the fuselage can be reduced to 35.82 m compared to an conventional design, resulting in a more favourable fuselage pitching moment.
The wetted area is increased compared to CeRAS CSR-01 with the same capacity and a round cross-section of the same height, as the increase from the larger cross-section circumference outweighs the reduction from the shortened fuselage (cf. Section 3.2.1). Nevertheless, HyZero's fuselage design offers aerodynamic advantages. On the one hand, the fuselage contributes to lift due to its wide design [21]. On the other hand, it increases aerodynamic efficiency due to its bell-shaped lift distribution. This allows for the narrower and lighter design of the wings, leading to fuel savings [16]. Another advantage is the guidance of the air along the fuselage, allowing the use of the BLI fan at the aft section (cf. Section 2.4.2). The geometric design of the tail-section is based on a study by Habermann [22]. Despite its streamlined design, the tail section offers sufficient space for the tank.

2.2.2. Windowless Fuselage

HyZero's design largely eliminates windows due to weight and overall fuel savings as well as reduced manufacturing costs [23]. Instead, OLED screens provide an outside view using small external cameras, complemented by infotainment content [24, 25]. The screens are clad in the traditional oval window design, which encourages passenger acceptance. For safety reasons, emergency exits continue to have windows in accordance with CS-25.809 [26].

2.3. Wing

HyZero's high-wing configuration, combined with the wing sweep of 8.2°, contributes to a negative sideslip-induced roll moment. To limit this moment and increase stability, an anhedral of 3° is chosen for the wing. Additional features of the wing are presented below.

2.3.1. High Aspect Ratio

In conventional aircraft, induced drag is responsible for roughly 35 % of overall drag [27]. Because the induced drag coefficient is inversely proportional to the aspect ratio for a finite wing, HyZero features a high-aspect ratio wing [28]. Conventional short-range aircraft, such as the reference aircraft, feature wing aspect ratios of 9 to 10. Modelled on the concept of Bradley [29], the optimum aspect ratio for a short-range aircraft with a configuration such as HyZero is set to 19.55. With $C_{D,i} = \frac{C_L^2}{\pi \cdot e \cdot AR}$, the selected aspect ratio results in a lift-induced drag reduction of 48.49 % compared to the reference aircraft, which leads to an overall drag reduction of about 17 % for a constant Oswald factor $e = 0.85$. The aspect ratio is limited for structural and airport logistic reasons. To avoid problems in ground handling because of the large wingspan, the wing tips can be folded upwards. The folding mechanism is a fail safe component, because the ailerons are located in the folding part and the wing does not provide enough lift without the outer sections. The mechanism leads to a 10 % mass increase due to additional components and structural reinforcements [30]. As the wing generates lift during flight, a higher wingspan has the disadvantage of a longer lever arm that exerts a higher bending moment onto the root. In addition, the thin wing can induce flutter motions during flight [31]. To reduce these unintended effects, a strut is added beneath the wing. The increase in both friction drag and mass is more than compensated by the reduction in induced drag [29], as further explained in Section 3.2.1.

2.3.2. Morphing Wing System

Since no fuel is stored in HyZero's wing, there is ample room for improvement of wing aerodynamics, including the installation of a morphing wing system. Traditional aircraft design aims to optimize aerodynamics and other factors with regard to a specific design point. As a result, operation under any other condition experienced during a mission is sub-optimal. With its morphing wing technology, HyZero can adapt to these different flight conditions.
The camber in an airfoil has significant impact on the generated forces. Camber variation is used to generate high lift coefficients [32]. In current aircraft, this is realized with the help of flaps, especially along the trailing edge. While highly effective for camber variation and area enlargement, flaps have several disadvantages. An abrupt change in camber results in an increase of drag over the baseline airfoil and can lead to an early flow separation at the trailing edge, limiting the maximum lift coefficient [33]. As flaps are independent components, separate from the wing, gaps in the surface are inevitable, causing drag and noise [34]. The morphing wing technology of HyZero solves these problems. The concept is derived from the Fishbone Active Camber (FishBAC) concept [33]. It is built around a highly anisotropic, compliant structural core with a pre-tensioned elastomeric matrix composite (EMC) skin. This allows for low part numbers which increases reliability, while combining a low chordwise stiffness with a high spanwise stiffness [35]. Wind tunnel testing confirms that the morphing system is able to increase the lift coefficient by $\Delta C_L = 0.72$ at $\alpha = 0°$, which is nearly identical to that of a 25 % chord flapped airfoil. The tests show a significant improvement in lift-to-drag ratio (L/D) of 20-25 % [33].

2.4. Hydrogen-Based Propulsion System

For HyZero's propulsion system, a parallel hybrid system of novel technologies is selected. A purely fuel cell-electric propulsion is disregarded due to the insufficient improvement in fuel cell technology anticipated until 2035. In particular, durability and reliability under flight conditions is a topic not sufficiently addressed by research [36].

Conventional turbofan engines are chosen as the main propulsors. They are complemented by the BLI fan, which is identified as a key technology for lifting body concepts like HyZero (cf. Section 2.2.1) [37]. The electric power for the aft BLI fan is provided by a fuel cell. Battery storage is kept as small as possible to only serve peak loads. A relatively low thrust is assigned to the BLI fan to harness the BLI benefit, while retaining larger and more efficient engines underneath the wings.

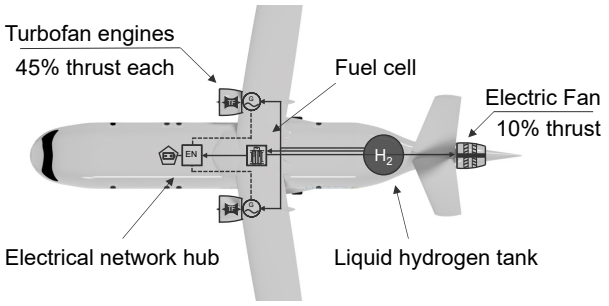

Figure 2. Overview of the drive train and major on-board systems

Figure 2 shows a schematic of HyZero's powertrain fitted to the NASA/DLR Design Challenge problem specification. In the following sections, the wing-mounted engines are discussed first, along with necessary adaptations to hydrogen. Then, the BLI fan is presented followed by on-board systems required for engine operation.

2.4.1. Wing-Mounted Engines

HyZero utilizes a high wing configuration with large ground clearances (cf. Figure 1), opening the possibility of fitting high-bypass ratio engines. Being a short- to medium-haul aircraft, only a limited time is spent in cruise flight. Therefore, design parameters are selected carefully to ensure an overall benefit.
A promising optimisation of under-wing engines is the boosted turbofan concept [38, 39]. Boosted turbofans allow greater flexibility of setting engine power, independent of the current thermodynamic operating conditions of the engine. However, the variations in thrust of a high-bypass turbofan engine at constant throttle already align well with the mission requirements at the different altitudes. This leaves little to be gained from the boosted turbofan concept, which would significantly increase aircraft weight [40]. Therefore, conventional gas turbines with the necessary adaptations to hydrogen fuel are selected.
A bypass ratio (BPR) of 14 is found to be optimal for future regional aircraft [41, 42]. To keep the outer diameter of the engine to a minimum, the core size needs to be reduced. This commonly reduces the thermodynamic efficiency of the core, due to lower channel height in the compressor. The blades need to be redesigned to deal with the resulting large relative tip clearance and low stability margin.
An extrapolation of remaining engine characteristics to 2035 is done based on engines with market entry between 2005 and 2020 with a thrust range of 90-150 kN. An overall pressure ratio (OPR) of 50 is set for the engine cycle. The last compressor stages are replaced by a radial stage to enable even lower channel heights [43]. A TSFC of 11.5 g/(kN s) is conservatively extrapolated for kerosene-fueled engines. The difference in heating value alone would put the equivalent TSFC for hydrogen at 4.12 g/(kN s). However, fuel consumption is even lower because of hydrogen's unique properties, as discussed in the following.
Running a conventional gas turbine on hydrogen requires design changes mainly for the burner injector. Micro-mix injection is used to enhance mixing by introducing interfering gaseous fuel and oxidizer jets. A side effect of a more homogeneous temperature distribution is lower thermal stress in the combustor, aided by the low emissivity of a hydrogen/air flame [11].
Generally, there is no carbon in fuel, thus eliminating CO_2 as a combustion product along with soot, unburned hydrocarbons, and carbon monoxide. The fuel is free of impurities to either erode or corrode the hot sections of the engine. However, hydrogen embrittlement is a major challenge [11]. The combustion products consist of water and a small amount of nitrogen oxides (NO_x). NO_x emissions can significantly be reduced due to the favourable properties of hydrogen. These include wide flammability limits, allowing lean combustion at lower temperatures, very high burning velocity, and high diffusivity minimising the dwell time of the reactants in hot areas [44, 45].
HyZero stores all necessary hydrogen at cryogenic temperatures. Prior to combustion, the fuel needs to be heated up to compressor exit temperatures to avoid severe efficiency losses. Hydrogen has a very high specific heat capacity, making it ideal for synergistic cooling applications in the engine. Starting at the front of the engine, precooling of compressor air promises to reduce the required compressor work and to increase OPR. However, benefits are limited especially for smaller engines. In addition, precooling poses many challenges, like the risk of ice formation and foreign object damage to the heat exchanger and is therefore dismissed [11, 46]. Instead, hydrogen is used to cool the turbine cooling air, thus lowering the cooling mass flow and increasing the thermodynamic efficiency. The turbine entry temperature (TET) can also be increased by at least 100 K [47], leading to benefits for many aspects of the engine. The energy that can be harnessed from cooling the turbine cooling air is insufficient for preheating the hydrogen. Therefore, an additional heat exchanger aft of the low-pressure turbine is added. The weight penalty is more than compensated by the reduction in fuel consumption [11].

2.4.2. Boundary Layer Ingesting Engine

In addition to the wing-mounted high-bypass engines, 10 % of cruise thrust is provided by the BLI fan shown in Figure 3. This share is set to the minimum value to harness large wake-filling benefits while limiting the weight increase of the aircraft. The BLI concept from

Ref. [48] uses a slightly lower thrust share for the BLI fan, owing to the larger aircraft. Another concept from Ref. [49] implements a relatively larger BLI system for a similarly sized aircraft, theoretically achieving even higher benefits. This is justified by the long range of the aircraft, where fuel consumption has a large influence on overall operational cost.

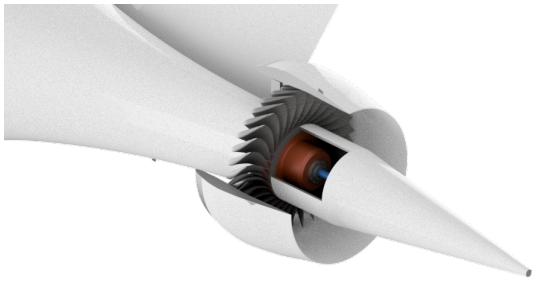

Figure 3. BLI fan mounted on the aft fuselage

As mentioned, the benefit from ingesting the slower boundary layer flow is the reduction in both jet and wake losses, resulting in lower overall thrust requirements [50]. Further benefits are a slight decrease in TSFC compared to the turbofan engines due to a more efficient, yet also heavier, drivetrain [51]. The BLI fan is positioned aft on the fuselage, as most viscous drag of an aircraft arises from the fuselage, especially for a lifting body [50]. A fully annular inflow is chosen to provide maximum benefit for a single-BLI fan configuration [50, 52]. Key parameters of the BLI fan are summarized in Table 3.

Table 3. Data of the BLI fan

Fan diameter	1.65 m
Cruise thrust	4 kN
Propulsive efficiency	0.9
Electrical efficiency	0.95
Cooling fluid	LH_2

A downside to utilising the boundary layer flow is a distorted inflow, resulting in performance loss of the BLI fan [53, 54]. However, for an axisymmetric inflow, the losses are minimal compared to one-sided BLI configurations [50]. Due to the low total pressure in the hub region, the fan root needs to be redesigned to yield any useful work. Moreover, the fan blade could operate near the design point in the clean flow area and stall as it travels through a disturbance from the wings, fuselage upsweep or the empennage [55].
Inlet guide vanes would be one option to homogenize the inflow [48]. They are not implemented in the final design due to weight considerations and possible future improvements in minimising the disturbances. The BLI fan operates at full load for most of the flight sections. The placement of the fan is not protected against foreign object damage. Therefore, the fan is shut off entirely on take-off and landing.

2.4.3. On-Board Systems

The hydrogen fuel is stored at cryogenic temperatures in tanks at the aft fuselage (cf. Section 2.1.1). The cryogenic hydrogen is used as a coolant for both the electric systems of the BLI fan, decreasing ohmic losses [56], and the fuel cell, recuperating waste heat.
A polymer electrolyte membrane (PEM) fuel cell is chosen for HyZero to supply electricity to on-board systems and the BLI fan. Advantages are a low overall weight, the capability to be scaled to size and a relatively quick response time to load changes [57]. This enables a small battery storage system to cover the load fluctuations. The necessary hydrogen for the fuel cell is supplied by two separate fuel lines. One of these extracts the hydrogen boil-off from the tanks. Since the boil-off rate is usually well below the fuel consumption rate, the second feed line carries LH_2 and is shared with one of the main engines. In general, both main engines are capable of being fed from each of the two tank compartments.
LH_2-carrying pipes need to be insulated to minimize heat leak into the fuel as well as to limit frost build-up and subsequent water accumulation inside the fuselage [37]. Analogous to the tank, foam insulation is chosen for its cost and safety benefits. Low-pressure fuel pumps are used in proximity to the tank, while main pumps are located close to the wing-mounted engines [11].
Operating a PEM fuel cell under flight conditions is a major challenge for current technology. First, the inlet air needs to be filtered for sulphur compounds as well as carbon monoxide to extend the service life of the fuel cell [58]. The low atmospheric pressure at cruising altitude is detrimental to fuel cell performance, requiring a more powerful compressor [59].
For emergency situations, the fuel cell is not an essential system as back-up power does not need to drive the BLI fan. 40 kWh of battery storage and emergency power from the main engines can cover the power need of essential systems.

3. TECHNICAL DATA

3.1. Mass Estimation

Table 4 shows the masses of the different components of HyZero. Most of them are calculated by semi-empirical equations, which were derived by Howe and Torenbeek [60, 61]. Since there are no semi-empirical equations for a wing like the one used by HyZero, the wing mass is adopted from a calculation for a similar aircraft [37].

3.2. Aerodynamic Data

For the analysis of aerodynamic effects, various software tools were used and will be cited when required.

3.2.1. Drag

A key factor in improving HyZero's aerodynamic efficiency is to keep drag at a minimum. To reach that

Table 4. Comparison of mass components in [kg]

Component	HyZero	Ref. aircraft
Fuselage	9 117 [60]	9 072 [60]
Wing	9 516 [37]	7 200 [15]
Empennage	539 [62]	896 [62]
Landing gear	1 736 [61]	2 633 [61]
Propulsion system	8 801 [15]	7 913 [15]
Tanks	1 090	–
Flight systems	4 145 [60]	4 247 [60]
Σ MME	34 944	31 961
Operating items	2 225 [60]	2 225 [60]
Furnishings	4 651 [61]	4 651 [61]
Σ OME	41 820	38 837
Payload	15 750	15 750
Block fuel	1 562	6 277
Σ MTOM	59 132	60 864

goal, a wide variety of features is incorporated, which are each explained in detail in Chapter 2. Due to the unconventional design, especially regarding the fuselage, the aircraft geometry tool OpenVSP is used to create a representative model for the drag analysis. For comparison, both HyZero and the reference aircraft are modelled in OpenVSP. For friction drag in laminar flow, the Blasius equation is used as described by White [63]. Several equations for turbulent flow are found in literature. To compare HyZero to the reference aircraft, the explicit fit equation of Spalding is used to compute friction drag in turbulent flows of both aircraft [64]. Figure 4 illustrates that the design choices of the HyZero concept lead to a small increase in zero-lift-drag ($C_{D,0}$).

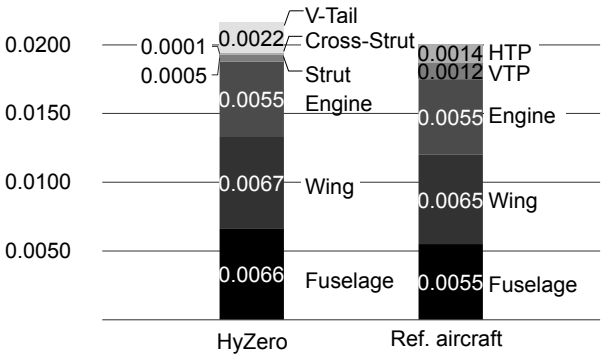

Figure 4. Zero-lift-drag comparison

The integration of a V-Tail reduces the drag of the empennage, which is the combination of vertical and horizontal tail plane (VTP and HTP) for the reference aircraft. The reduction is mainly caused by the decreased empennage-fuselage interference drag and in parts also by a slight reduction in wetted area. Due to the lifting fuselage design, the increase in length caused by the integration of the tank can be kept at a minimum; this, in turn, limits the increase in fuselage drag.

HyZero features an airfoil that is designed for natural laminar flow (NLF). In historic commercial aircraft of similar size, the boundary layer flow is turbulent across most of the wetted surface. This results in viscous drag five to ten times larger than that of laminar boundary layers [65]. The NASA/LANGLEY NLF(1)-0215F airfoil is determined as a suitable fit since it provides a high $C_{L,\,max}$, while maintaining a low C_D over a wide range of C_L. At the flight conditions of the standard HyZero mission (cf. Section 5), laminar flow is maintained for 48.83 % of chord length in a calculation with the analysis tool XLFR5. This corresponds with data found by Streit [66], who maintains laminar flow for up to 50 % chord length with an NLF airfoil at $Ma = 0.78$ and $Re = 1.4 \cdot 10^7$. The laminar flow length for the reference aircraft is estimated to be 20 % of the lifting surfaces chord length, as is the case with most similar short- to medium-range aircraft [15]. Laminar flow helps keeping $C_{D0,\,wing}$ at a value comparable to the reference aircraft despite an increased wetted area.

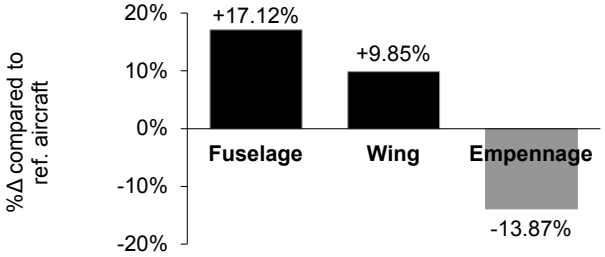

Figure 5. Zero-lift drag compared to the reference aircraft

A visualisation of the difference in zero-lift drag compared to the reference aircraft is given in Figure 5. The morphing wing concept (cf. Section 2.3.2) further reduces the overall drag coefficient by approximately 3.7 % [67].

The drag share for the lifting body fuselage contributes 27% of overall drag. The BLI fan, positioned at the rear of the fuselage, ingests the lower 40 % of the boundary layer, equalling to 65 % of the momentum deficit of the fuselage due to the nonlinear velocity curve of a typical boundary layer [49]. At $C_{L,\,cruise}$, the ratio of viscous drag to total drag is 83 %, as induced drag is low due to the high aspect ratio and wave drag is neglected at cruise conditions. This results in a power saving coefficient of 4 % according to Steiner [68], which can roughly be translated into an equal overall drag reduction.

As discussed in Section 2.3, the high aspect ratio of HyZero's wing also reduces lift-induced drag. The glide ratio of HyZero exceeds that of the reference aircraft at very low values of C_L. However, the glide ratio finds its maximum at $C_L = 1.1$, partly due to the very high aspect ratio. This is much higher than $C_{L,\,cruise} = 0.5$. In the course of optimisation, it was considered to lower the aspect ratio. However, even for significantly lower aspect ratios, which have their $(L/D)_{max}$ at values closer to $C_{L,\,cruise}$, the glide ratio

of HyZero at $C_{L,\,cruise}$ exceeds those of lower aspect ratios substantially. This shows that the HyZero concept is superior to others even in non-optimal flight conditions. To fully utilize its potential, it could be considered to fly at a lower speed. Due to the TLARs this is not explored further in this work. Overall, HyZero achieves an increase in (L/D) at $C_{L,\,cruise}$ of 4.6 % and an increase in $(L/D)_{max}$ of 40.9 %.

3.2.2. Lift

As discussed above, an airfoil for natural laminar flow is used for the wing. For computing a $C_L - \alpha$ curve, the airfoil's behaviour is analyzed at HyZero's average chord length of 2.56 m with a Reynolds number of $Re = 6.78 \cdot 10^6$ at $Ma = 0.7$ with MSES. To apply the 2D data to the behaviour of a 3D wing, 2D-3D transformations usually have to be made. As the sweep of HyZero's wing is rather small, $C_{L,\,3D}$ would not differ significantly from $C_{L,\,2D}$. For that reason, 3D transformation is neglected.
Lift is also increased by the lifting fuselage design. The contribution of fuselage lift to the total lift coefficient can be estimated to 20 % of overall lift as investigated by Drela [21]. The high-lift system is sized according to Stumpf [15], Scholz [69] and CS-25.125 [26] to achieve a reference speed V_{ref} of 130 kt and a take-off field length (TOFL) of less than 2 000 m. HyZero can achieve V_{ref} at MTOM for safety reasons. To simplify calculations regular high-lift components are assumed rather than the morphing wing. The high-lift system therefore comprises of a droop nose or nose flaps at the leading edge and a plain flap at the trailing edge for calculation purposes. In landing configuration HyZero uses a 25° slat and 35° flap deflection angle to achieve a lift coefficient $C_L = 2.23$.

4. AIRPORT AND HYDROGEN INFRASTRUCTURE

The introduction of new aircraft designs is hindered by the need to adapt aircraft infrastructure. Hydrogen aircraft in particular potentially require an entirely new fuel procurement chain, infrastructure, and procedures.
HyZero is designed to largely avoid these issues. It fits within current gate operations without requiring major changes to infrastructure or procedures. The hydrogen procurement chain is developed from the options listed in Figure 6 with the goal of requiring the least investment and adjustments from airport operators. The path highlighted in gray is selected.
In the following sections, the assumptions and calculations supporting the selected hydrogen procurement chain are described in detail. All costs are in EUR_{2035} unless specified otherwise, assuming a 2 % annual inflation between 2021 and 2035 as targeted by the European Central Bank [63].

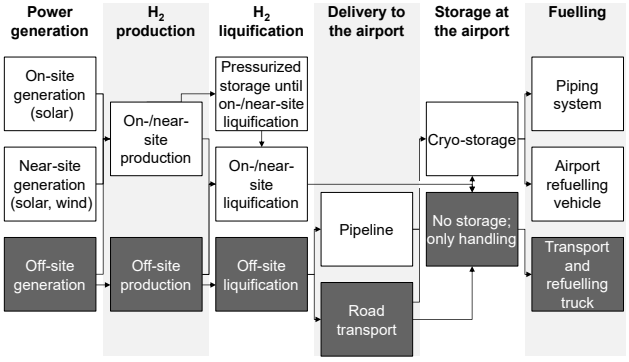

Figure 6. Potential and selected LH_2 procurement chain.

4.1. Power Generation

HyZero is powered by 'green' hydrogen, i.e. hydrogen produced exclusively with energy from renewable sources [70]. To encourage the production of green hydrogen, the German Federal Government is providing extensive incentives to industrial electrolysers. These include exemptions from the EEG surcharge, which finances the expansion of renewables in Germany, and the German electricity tax, as well as reimbursements for the grid charge in the first 20 years of their operation. Considering these exemptions, the price of electricity for electrolysers in 2020 is estimated at $0.069\,\mathrm{EUR}_{2020}/\mathrm{kWh}$ [70–74]. Given the ever-decreasing cost of electricity from renewable sources, and the expressed intend of the German Federal Government to keep electricity prices for the generation of hydrogen low, the price of electricity for electrolysers is assumed to remain constant at an inflation-adjusted $0.093\,\mathrm{EUR}_{2035}/\mathrm{kWh}$ until 2035 [75].

4.2. Hydrogen Production

Large-scale electrolysis plants benefit from the above incentives and efficiency improvements when compared to smaller facilities. The hydrogen for HyZero's operation is therefore produced at a centralized, off-site location [70, 76]. Electrolysis splits water into hydrogen and oxygen using electricity and one of three process variants: alkaline electrolysis (AEL), polymer electrolyte membrane electrolysis (PEMEL), or high-temperature electrolysis (HTEL) [74]. The technology readiness levels (TRL) of these technologies are 9, 6-8, and 5-6, respectively, with 9 indicating a proven status [74, 77].
AEL is primarily used for producing hydrogen on an industrial scale today and features the lowest production costs [78]. Drawbacks include the lack of purity of the produced hydrogen, which necessitates an additional filtering step, and the limited ability of the process to adapt to a fluctuating electricity supply from renewable sources. [79, 80] PEMEL is less well-established, but seen as having a higher potential for future improvement [81], including significant efficiency, compactness, and production capacity advantages over AEL [82–84]. PEMEL can dynamically adapt its production rate between 0 % and 300 % of its

nominal power rating, far exceeding the capabilities of AEL and HTEL [80]. It therefore offers the potential for demand-side management, which is seen as an important factor in realising the transformation of global energy supplies to 100 % renewable sources [85]. HTEL prototypes are being operated in laboratory environments and only a few, small-scale demonstrators have been implemented. The advantages of HTEL are its high efficiency, reduced CapEx, and its ability to be operated 'in reverse' to produce electricity from hydrogen [86, 87]. Drawbacks include HTEL's inflexibility, the still unknown purity of the hydrogen produced on an industrial scale, and, most importantly, the uncertainty regarding its availability for large-scale hydrogen production in 2035 given its relatively low TRL [78, 83]. Because of these uncertainties, the option of using HTEL is dismissed and excluded from the following cost calculations. When comparing the economics of AEL and PEMEL, initial investment, cost of electricity, maintenance, and electrolysis stack renewal cost are major cost components that need to be considered.
All cost components can be annualized over the expected lifetime of the plant, according to Equations 1 and 2 [88]:

$$c_{annualized} = CRF \cdot c_{NPC}, \tag{1}$$

$$CRF = \frac{i \cdot (1+i)^N}{(1+i)^N - 1}. \tag{2}$$

Using a real discount rate of $i = 0.04$ and an expected lifetime of both systems of $N = 23$ years [84], the common capital recovery factor is $CRF = 0.067$. Calculations for the net present cost c_{NPC} assume initial investment costs of around 700 EUR/kWh for large-scale AEL and 980 EUR/kWh$_{el}$ for large-scale PEMEL plants [83]. The average electrolysis plant supplying HyZero in 2035 is assumed to have a nominal power P_{el} of 100 MW, based on literature, detailed plans by European companies, and a call for proposals by the European Commission [89–91]. Annual maintenance and operations costs are estimated at 22 EUR and 8 EUR per kW of installed power per year for a 100 MW AEL and PEMEL plant, respectively [78]. The lifetimes of the individual electrolysis stacks are estimated at 60 000 and 50 000 hours, respectively [78, 92]. The capacity factors CF are 90 % and 70 % for AEL and PEMEL, respectively. The values are chosen to account for the high TRL of AEL and the key advantage of PEMEL, which lies in its ability to change its power level according to the supply of renewable energy.
Table 5 summarizes the calculated results for the net present cost in 2035, annualized cost, and cost per kg of hydrogen.
The cost per kg of hydrogen is determined by dividing the annualized cost by the annual production, which is derived from Equation 3:

$$m_{H2,annual} = \frac{P_{el} \cdot CF \cdot 8\,760\,{}^{h}/_{a}}{LHV_{H2}} \cdot \eta_{system}. \tag{3}$$

Table 5. Production cost per kg of hydrogen.

	AEL	PEMEL
c_{NPC} (2035) [mn EUR]	1 204	974
Annualized cost [mn EUR]	80.73	65.26
Annual production [t_{H2}]	20 124	14 731
Production cost [EUR/kg_{H2}]	4.01	4.43

The electric power P_{el} and capacity factors CF are given above. The lower heating value of hydrogen LHV_{H2} is 33.3 kWh/kg_{H2}. The system efficiency of AEL and PEMEL electrolysis is 85 % and 80 %, respectively [86].
Utilizing AEL results in a 9 % cost advantage per kilogram of hydrogen over PEMEL. However, PEMEL's major advantage is its compatibility with electricity from variable, renewable sources. This compatibility is represented within the calculations in the form of the significantly lower capacity factor and is responsible for a significant part of PEMEL's cost disadvantage. The ability to use the electricity from variable renewable sources guarantees that HyZero's hydrogen is truly 'green'. PEMEL therefore provides the best balance between ecology, cost, and technology-specific advantages for implementation in 2035, and is selected as the optimal technology for producing HyZero's hydrogen.

4.3. Hydrogen Liquefaction

Similar to hydrogen production, large-scale, centralized hydrogen liquefaction offers efficiency and cost advantages over an on-site process and is therefore selected for procuring HyZero's hydrogen [76]. An energy demand of 9 kWh/kg_{H2} is chosen as a reasonable estimate for a large-scale liquefaction plant in 2035 [76,93]. The specific cost of hydrogen liquefaction is calculated using Equation 4:

$$c_{spec,liq} = c_{spec,I\&O} + e_{spec,liq} \cdot c_{el,green}. \tag{4}$$

Conelly et al. [93] estimate a specific cost of investment and operations $c_{spec,\,I\&O}$ of around 1.19 EUR_{2018}/kg_{H2} for liquefaction plants with a production capacity of 27 t_{H2}/day in California in 2018. The investigated PEMEL plant's annual production of 14.73 mn kg_{H2} translates into roughly 40 t_{H2} per day. Assuming this to be the output of a liquefaction plant directly connected to the PEMEL plant, and considering a plant built in Germany instead of California, as well as the likelihood of further technological improvement until 2035, a specific cost of investment and operations of the liquefaction plant of 1.00 EUR/kg_{H2} is a reasonable assumption. Using the aforementioned specific energy demand $e_{spec,\,liq}$ of 9 kWh/kg_{H2} and the estimation for the cost of green electricity in 2035 $c_{el,green}$ from Section 4.1, the specific cost of liquefaction is calculated to $e_{spec,\,liq} = 1.84$ EUR/kg_{H2}.

4.4. Delivery to the Airport

The use of pipelines for transporting LH_2 to airports is dismissed because of the high costs and operational requirements [94]. HyZero relies on LH_2 being delivered by cryogenic trucks, which can utilize existing, proven technologies and can be scaled easily as HyZero expands to more airports. Existing cryogenic semi-trailers carry up to 4 000 kg of hydrogen for up to 4 000 km [95–97]. The total cost of ownership (TCO) of a hydrogen-powered cryogenic semi-trailer is estimated at 2.00 EUR/km based on work by Oostdam [98] and estimates for the cost of a hydrogen cargo tank and auxiliary equipment [96]. For the calculation of transportation cost, a mean distance of 200 km is assumed. Assuming a conservative average speed of the truck of 50 km/h and hourly personnel cost of 25 EUR, the cost of the driver for the 400 km roundtrip is $c_{driver} = 200$ EUR. Once at the airport, the truck is transferred to airport personnel.
Daily hydrogen requirements per airport amount to 10 512 kg_{H2} based on three stationed aircraft with an average of 4.3 flights (2.05 flights at 2000 km and 2.25 flights at 600 km) per day (cf. Section 5.2). This requires three trips by hydrogen-delivery trucks, each filled with an average of 3 504 kg_{H2}. The boil-off in a truck is 0.0125 % per hour and needs to be considered when filling the truck at the liquefaction plant [96]. Transportation time is conservatively estimated at four hours, and another hour is included for possible delays. Since the delivery trucks are used to directly fuel the aircraft, they remain at the airport until they have dispensed their fuel completely. With an average demand per flight of around 817 kg_{H2}, each truck is involved in five fueling operations, on average. Assuming the average 12.9 HyZero flights per airport per day to be equally spaced between 5:30 am and 11 pm, this means each truck must remain at the airport for an average of six hours and 45 minutes. Another five hours of storage time within the truck are included for potential departure delays, as only a negligible number of flights in the EU are delayed by more than 300 minutes [99]. The maximum boil-off duration is therefore 16.75 hours, which corresponds to a maximum boil-off of 0.2 % or around 7 kg_{H2}. This puts the average total hydrogen mass per delivery at 3 511 kg_{H2}. However, the additional 7 kg_{H2} are not considered when calculating the specific delivery cost, as in most cases, they are not used to fuel HyZero but rather remain inside the truck and are recycled at the liquefaction plant. More significant are the transfer losses (cf. Section 4.5), which amount to an average of 70 kg_{H2} per truck, putting the total amount of hydrogen used for calculating the specific cost of transportation at 3 574 kg_{H2} [100]. The final specific cost of transportation is calculated to 0.28 EUR/kg_{H2} using Equation 5:

$$c_{spec,trans} = \frac{c_{spec,TCO} \cdot d_{mean} + c_{driver}}{m_{H2}}. \tag{5}$$

4.5. Fueling and Gate Operations

A significant source of hydrogen boil-off is transfer loss from the receiving tank, which amounts to about 2 % for a transfer process using low-pressure transfer pumps and is considered in the Direct Operating Cost (DOC) calculations (cf. Section 5.3) [100]. To minimize its environmental and cost impact, the boil-off is recovered from the tanks' pressure release vents and fed into the fuel cell powering the delivery and fueling truck. Other than that, gate operations require little adjustments. Fueling of HyZero takes place between passenger off- and on-boarding. Other turnaround processes can take place simultaneously, as hydrogen aircraft handling is not expected to be more dangerous, especially considering the technological advances until 2035 [101, 102]. In its 'wingtips-up' configuration, HyZero falls within the ICAO wingspan limit of 36 m (cf. Figure 1) [103]. The positioning of the main engines below the wings and the BLI engine in the aft section allow it to utilize existing infrastructure for ground operations and maintenance. During the night, the unused diversion fuel from the final flight of the day remains in HyZero's tank. This avoids excessive thermal cycling and reduces boil-off during the first fueling in the morning [100].
By using hydrogen delivery trucks equipped with direct fueling capabilities, the need for expensive infrastructure, especially tanks, is all but eliminated. Changes that cannot be avoided are the installation of additional venting in hangars for maintenance, and the implementation of additional training and procedures for the safe handling of hydrogen, due to its volatility. [104]

4.6. Total Cost of Hydrogen Procurement and Efficiency Assessment

Table 6 lists the cost components of HyZero's hydrogen, given the calculations and assumptions detailed above. A 10 % markup on the total cost is assumed to account for supplier margins. This puts the total specific cost of hydrogen for HyZero's operation at 7.21 EUR/kg_{H2}.

Table 6. Summary of specific cost components of HyZero's hydrogen.

	Specific cost [EUR/kg_{H2}]
H_2 production	4.43
H_2 liquification	1.84
H_2 delivery	0.28
Σ Sum	6.55
Total w/ markup	7.21

For the total energy assessment, a top-down approach, based on the efficiency values provided by the NASA/DLR Design Challenge problem specification, is utilized. The efficiency of electrolysis is given as $\eta_{electrolysis} = 0.80$, and that of liquefaction, distribu-

tion, and storage, which is assumed to include fueling, as a combined $\eta_{liq,\,distr,\,sto} = 0.85$. Since the electricity for hydrogen production and liquefaction stems from renewable sources, the efficiency of electricity generation is $\eta_{el} = 1$. The total onboard efficiency from hydrogen tank to thrust in cruise is shown to be around $\eta_{onboard} = 0.43$, neglecting the impact of the fuel cell and BLI engine. The total efficiency of the hydrogen chain from electricity generation to thrust is therefore approximately $\eta_{total} = 0.29$.

5. OPERATIONAL ASPECTS

Based on HyZero's configuration, the mission profile is optimized with regard to climate impact, fuel consumption, and noise. For certain aspects, like determining the required tank size, the block fuel is relevant which includes the trip fuel and all reserves, as defined by EU-OPS 1.255 [105]. For economic evaluations the trip fuel is investigated, which excludes reserves.

5.1. Flight Path Optimization

While HyZero does not emit any CO_2 or CO (cf. Section 2.4) during its flight, its emission of H_2O and thus the potential to produce contrails is greatly increased compared to kerosene-fueled aircraft. In addition, NO_x is emitted, albeit at reduced levels. The level and impact of these emissions is greatly influenced by HyZero's flight path. HyZero's mission profile it designed to be as environmentally friendly as possible. In addition, its economic viability is investigated.

5.1.1. Climate Impact from Greenhouse Gases

To reduce the climate impact of both reference missions, the greenhouse gas (GHG) emissions of HyZero are studied to determine it's climate impact. Counterintuitively, GHG emission and climate impact can show an inverse correlation. For example, at lower altitudes, HyZero has a higher fuel consumption and thus emits more H_2O, but nevertheless has a lower climate impact due to atmospheric effects. The latter can be measured using several different metrics [104]. The CO_2-equivalent (CO_2-eq) metric is chosen, as the values needed to calculate it are readily available. CO_2-eq is calculated by multiplying each GHG emission with its respective global warming potential (GWP) and adding them all up to obtain the total CO_2-eq or climate impact. GWP represents which amount of CO_2 would have the same time-integrated radiative forcing (RF) as the GHG under consideration. For this work, the widely accepted standard time horizon of 100 years is chosen [106].
Due to the previously described contrary effects of cruising altitude and climate impact, a trade-off is necessary when choosing the cruising altitude. An investigation into the optimal cruising altitude is conducted for HyZero.
The climate impact of contrails is between three [107] and ten times [108] as high as that of all GHG emission in aviation. Although studies have argued that contrails produced by aircraft fueled with LH_2 are less harmful, e.g., due to being optically thinner [109], HyZero still flies below FL 300 to not produce any contrails at all [104]. The CO_2-eq and fuel burn is analyzed across different FLs for HyZero. The CO_2-eq from GHG emissions is already greatly reduced below FL 300 and NO_x is the only remaining GHG which possesses a GWP. While the GWP of NO_x continues to decrease below FL 300, the fuel consumption rises, leading to an overall stagnation in CO_2-eq. Therefore, the cruising altitude of HyZero is set at FL 290, as this is the cruising altitude with no contrail formation and least fuel consumption. The CO_2-eq of the 600 km mission is 164.04 kg and of the 2 000 km mission 654.3 kg. The CO_2-eq is 33 times lower than that of the reference aircraft. It is evident that HyZero has an extremely low climate impact.

5.2. Fuel Consumption Analysis

The calculation of the fuel consumption is conducted for the block fuel of the 2 000 km mission. Through the configuration decisions detailed in previous chapters, HyZero consumes 34-41 % less energy on every mission evaluated. Including all reserves, HyZero requires 1 561.5 kg of block fuel on the 2 000 km mission. This is the dimensioning figure for the tank size. The fuel masses for all missions are summarized in Table 7. The taxi fuel and a delay of 15 minutes on 20 % of flights is included in the trip fuel to achieve more robust results. It can be seen that the difference between trip fuel and block fuel is a closer for HyZero than the reference aircraft due to the low mass penalty of carrying LH_2.

Table 7. Overview of fuel masses in [kg]

	HyZero	Ref. aircraft
Trip fuel 2 000 km	1 129.2	4 777.1
Block fuel 2 000 km	1 561.5	6 961.8
Trip fuel 600 km	533.7	2 130.8
Block fuel 600 km	936.8	4 183.3

As laid out in Section 2.1.2, HyZero does not utilize removable tanks to realize weight reductions for the shorter 600 km mission, as the drawbacks outweigh the benefits. This design decision opens an opportunity aligned with HyZero's mission of accessing a growing number of airports without requiring significant investments from airport operators. HyZero's standard operating model of delivering LH_2 to airports via trucks might not be feasible for all locations. If these airports are within 600 km of an airport with refueling capabilities, operators could still trial new HyZero routes without committing to significant investments. HyZero could service these airports by utilising its entire tank capacity designed for the 2 000 km mission and carrying the return fuel on the outbound flight, removing the need for refueling at the destination. The capacity is sufficient to allow the aircraft to respect

all requirements regarding reserve fuel. HyZero could remain in holding for up to 30 minutes during the outbound flight. Only if this time, which represents about 30 % of the trip time, were to be exceeded, HyZero could not operate the return flight. In these rare cases, LH_2 would need to be supplied on-demand. This risk seems acceptable, given the potential for significant expansion of business.

5.3. Direct Operation Cost Analysis

Both reference missions are considered for creating an average HyZero mission for the DOC analysis. Aircraft generally do not operate exclusively on either a 600 km or a 2 000 km mission. Therefore, HyZero's block time and daily flight numbers are based on the average of all US narrowbodies [110]. In 2019, these had an average daily block time of 9.95 hours and operated 4.3 daily flights. This leads to a daily frequency of 2.05 and 2.25 of the 2 000 and 600 km mission, respectively, and an average HyZero mission distance of 1 266.6 km.
The DOC analysis is carried out based on the same method as employed by CeRAS [3]. Unless specified otherwise, the same input values are used for the DOC as those set out by Franz [111]. If costs change with the type of flight and/or region, an international flight within the EU is assumed. All equations are adjusted to account for any changes in aircraft configuration like an additional engine. For the price of hydrogen fuel, the price calculated in Section 4.6 to 7.21 EUR/kg_{H2} is used. To account for boil-off losses during fueling 2 % of fuel consumption is added.
A price of 0.69 EUR/l for JET A-1 [112] is assumed and 2.64 EUR/l for SAF [113]. With a 30 % SAF blend this leads to a fuel price of 1.60 EUR/kg for the reference aircraft. The fuel costs of the reference aircraft are further increased by the cost of CO_2 pricing. The price of CO_2 emissions is projected at 112.2 EUR/t_{CO2} under the EU-Emissions Trading Scheme (EU-ETS). [114] The purchase price of both aircraft is estimated using Kundu [62] and calibrated with a A319neo from Airbus [115].This results in a list price for HyZero of 95.6 mn EUR.
The results of the DOC analysis are presented in Figure 7. It can be seen that total the DOC of HyZero are significantly higher due to the high fuel costs. For both aircraft, the fuel costs account for the majority of DOC. On the one hand, a separate sensitivity analysis shows that a 20 % decrease in the price of LH_2 decreases the total DOC of HyZero by 14.2 %. On the other hand, the total DOC of the reference aircraft would rise by 25.4 % if it was only fueled with SAF. Another observation is that HyZero has lower fees, as they are directly correlated to the aircraft's MTOM.
Overall, the DOC of both HyZero and the reference aircraft are greatly influenced by political and macroeconomic factors and the projected DOC are therefore expected to change with changing circumstances. Currently, hydrogen prices appear prohibitively high which should change with advances in hydrogen production technology. In addition, the EU Commission has proposed to price non-CO_2 emissions in the future, further negatively impacting the reference aircraft [116].

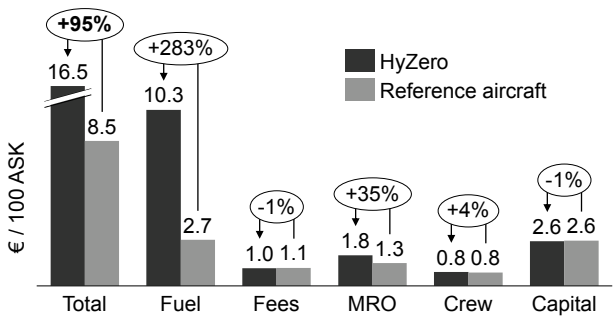

Figure 7. DOC comparison

6. CONCLUSION

As required by the problem formulation of the NASA/DLR Design Challenge 2021, HyZero carries 150 passengers over a maximum distance of 2 000 km and thus competes with other short- to medium-haul aircraft. For this reason, HyZero is compared with an updated CeRAS CSR-01 with improved engines, which are at a similar technology level. Therefore, their fuel consumption has been extrapolated for the use in 2035.
HyZero's configuration features a high-aspect ratio wing supported by a strut, providing reductions in fuel consumption. The two main engines, which combust hydrogen, are located under the wing, mounted high on the fuselage. In addition, a BLI fan at the end of the fuselage, which is power by a fuel cell system, ingests the boundary layer, increasing the propulsive efficiency. Other striking features of the HyZero include a V-tail and a windowless fuselage, resulting in reduced fuel consumption through mass savings. In addition, the wings are designed to be foldable in order to fit within conventional 36 m airport boxes. The use of morphing wings reduces not only the drag but also noise. A mass estimation of both aircraft and their system components demonstrates HyZero's competitiveness.
Green house gas emissions are decreased significantly compared to the reference aircraft, because of the use of hydrogen as fuel, with its entire procurement chain being focused on sustainability. As a result, HyZero only emits NO_x and water vapor. HyZero meets the TLARs of the NASA/DLR Design Challenge 2021, making it an environmentally friendly alternative for air transport in 2035.

Contact address:

sekretariat@ilr.rwth-aachen.de

References

[1] European Commission. Commission Staff Working Document Impact Assessment. In Commission Staff Working Document Impact Assessment. European Commission, Brüssel, 2020.

[2] German Aerospace Center. White Paper Zero Emission Aviation, 2020.

[3] Kristof Risse, Katharina Schäfer, Florian Schültke, and Eike Stumpf. Central Reference Aircraft data System (CeRAS) for research community. CEAS Aeronautical Journal, 7(1), March 2016.

[4] S. Andersson, J.and Grönkvist. Large-Scale Storage of Hydrogen. International Journal of Hydrogen Energy, 2019.

[5] E. Rivard, M. Trudeau, and K. Zaghib. Hydrogen Storage for Mobility: A Review. Materials, 2019.

[6] T. Brunner, O. Kircher, and M. Kampitsch. Cryo-Compressed Hydrogen Storage. In Fuel Cells : Data, Facts and Figures. John Wiley & Sons, Ltd, 2016.

[7] H. Thanh and et al. Technical Assessment of Compressed Hydrogen Storage Tank Systems for Automotive Applications. Technical report, Argonne National Laboratory - Nuclear Engineering Division, Chicago, 2010.

[8] H. Pohl. Hydrogen and Other Alternative Fuels for Air and Ground Transportation. John Wiley & Sons Ltd, Michigan, 1995.

[9] Airbus S.A.S. These pods could provide a blueprint for future hydrogen aircraft, 2020.

[10] N. Dangi and A. Patel. Simulated Drag Study of Fuel Tank Configurations for Liquid Hydrogen-Powered Commercial Aircraft. SAE International Journal of Sustainable Transportation, Energy, Environment, & Policy, 2020.

[11] G. Brewer. Hydrogen Aircraft Technology. Routledge, Boca Raton, 1991.

[12] C. Winnefeld, T. Kadyk, B. Bensmann, U. Krewer, and R. Hanke-Rauschenbach. Modelling and Designing Cryogenic Hydrogen Tanks for Future Aircraft Applications. Energies, 2018.

[13] P. Sharke. H2 Tank Testing. Mechanical Engineering-CIME, 2004.

[14] D. Verstraete. The Potential of Liquid Hydrogen for Long Range Aircraft Propulsion. PhD thesis, Cranfield University, 2009.

[15] E. Stumpf. Vorlesung Flugzeugbau II Sommersemester 2021 exercises 5,7,11. 2021.

[16] V. Mukhopadhyay, J. Welstead, J. Quinlan, and M. Guynn. Structural Configuration Systems Analysis for Advanced Aircraft Fuselage Concepts. Washington, D.C., 2016. American Institute of Aeronautics and Astronautics.

[17] International Air Transport Association. Aircraft Technology Roadmap to 2050, 2020.

[18] A. Velicki and D. Jegley. PRSEUS Development for the Hybrid Wing Body Aircraft. Virginia Beach, 2011. American Institute of Aeronautics and Astronautics.

[19] V. Mukhopadhyay and M. Sorokach. Composite Structure Modeling and Analysis of Advanced Aircraft Fuselage Concepts. Dallas, 2015. American Institute of Aeronautics and Astronautics.

[20] J. Chambers, B. Yutko, R. Singh, and C. Church. Structural Optimization Study of the D8 Double-Bubble Composite Fuselage. Grapevine, 2017. American Institute of Aeronautics and Astronautics.

[21] M. Drela. Development of the D8 Transport Configuration. Honolulu, 2011. American Institute of Aeronautics and Astronautics.

[22] International Air Transport Association. Technology Roadmap for Environmental Improvement, 2020.

[23] S. Steinke. Emirates führt virtuelle Fenster ein. Flugrevue, 2017.

[24] S. Bagassi, F. Lucci, and F. Persiani. Aircraft Preliminary Design: A Windowless Concept. CEAS, 2015.

[25] M. Moruzzi and S. Bagassi. Preliminary Design of a Short-Medium Range Windowless Aircraft. International Journal on Interactive Design and Manufacturing (IJIDeM), 2020.

[26] European Union Aviation Safety Agency. Certification Specifications for Large Aeroplanes (CS-25). Amendment 26, 2020.

[27] E. Stumpf. Vorlesung 6 widerstand Flugzeugbau I Wintersemester 2020/21. 2019.

[28] J. Anderson. Fundamentals of Aerodynamics. McGraw-Hill, New York, 1991.

[29] M. Bradley, C. Droney, and T. Allen. Subsonic Ultra Green Aircraft Research: Phase II – Volume I – Truss Braced Wing Design Exploration. Technical report, National Aeronautics and Space Administration, Boeing Research and Technology, Huntington Beach, 2015.

[30] Yarygina, M. V. and Popov, Yu. I. Development of the Weight Formula for a Folding Wing. Technical report, Moscow Aviation Institute (State Technical University), Moscow, 2011.

[31] V. Rozov, A. Hermanutz, C. Breitsamter, and M. Hornung. Aeroelastic Analysis of a Flutter Demonstrator With a Very Flexible High-Aspect-Ratio Swept Wing. Como, 2017.

[32] D. Raymer. Aircraft Design: A Conceptual Approach. American Institute of Aeronautics and Astronautics, Inc, Reston, 2018.

[33] B. Woods, O. Bilgen, and M. Friswell. Wind Tunnel Testing of the Fish Bone Active Camber Morphing Concept. Journal of Intelligent Material Systems and Structures, 2014.

[34] J. Delfs and L. Enghardt. Latest research on the reduction of aircraft noise at the source, 2013.

[35] B. Woods and M. Friswell. Preliminary Investigation of a Fishbone Active Camber Concept. Stone Mountain, 2012. ASME.

[36] N. Dyantyi, A. Parsons, C. Sita, and S. Pasupathi. PEMFC for Aeronautic Applications: A review on the Durability Aspects. Open Engineering, 2017.

[37] M. Bradley. Subsonic Ultra Green Aircraft Research Phase II: N+4 Advanced Concept Development. NASA, 2012.

[38] M. Hoogreef, R. Vos, R. de Vries, and L. Veldhius. Conceptual Assessment of Hybrid Electric Aircraft with Distributed Propulsion and Boosted Turbofans. AIAA Scitech 2019 Forum, 2019.

[39] T. Hecken and et al. Conceptual Design Studies of "Boosted Turbofan" Configuration for Short Range. In AIAA Scitech 2020 Forum. American Institute of Aeronautics and Astronautics, Reston, 2020.

[40] National Academies of Sciences, Engineering and Medicine. Commercial Aircraft Propulsion and Energy Systems Research: Reducing Global Carbon Emissions. The National Academy Press, Washington, 2016.

[41] L. Wiart, O. Atinault, R. Grenon, B. Paluch, and D. Hue. Development of NOVA Aircraft Configurations for Large Engine Integration Studies. Reston, 2015. AIAA.

[42] D. Daggett, S. Brown, and R. Kawai. Ultra-Efficient Engine Diameter Study, 2003.

[43] F. Lou and N. Key. Design Considerations for the Final-Stage Centrifugal Compressor in Aeroengines. Journal of Propulsion and Power, 2020.

[44] B. Khandelwal, A. Karakurt, P. Sekaran, V. Sethi, and R. Singh. Hydrogen Powered Aircraft : The Future of Air Transport. Progress in Aerospace Sciences, 2013.

[45] H. Lei and B. Khandelwal. Investigation of Novel Configuration of Hydrogen Micromix Combustor for Low NOx Emission. In AIAA Scitech 2020 Forum. American Institute of Aeronautics and Astronautics, Reston, 2020.

[46] I. Van Dijk, A. Roa, and J. van Buijtenen. Stator Cooling and Hydrogen Based Cycle Improvements. Int. Soc. of Air Breathing Engines 2009, 2009.

[47] A. Jackson. Optimisation of Aero and Industrial Gas Turbine Design for the Environment. PhD thesis, Cranfield University, 2009.

[48] A. Seitz and et al. Proof of Concept Study for Fuselage Boundary Layer Ingesting Propulsion. Aerospace, 2021.

[49] J. Welstead and J. Felder. Conceptual Design of a Single-Aisle Turboelectric Commercial Transport with Fuselage Boundary Layer Ingestion. Cleveland, 2016. NASA Glenn Research Center.

[50] A. Uranga and et al. Boundary Layer Ingestion Benefit of the D8 Transport Aircraft. AIAA Journal, 2017.

[51] P. Giannakakis, Y. Maldonado, N. Tantot, C. Frantz, and M. Belleville. Fuel Burn Evaluation of a Turbo-Electric Propulsive Fuselage Aircraft. In AIAA Propulsion and Energy 2019 Forum. American Institute of Aeronautics and Astronautics, Reston, 2019.

[52] L. Wiart and C. Negulescu. Exploration of the Airbus Nautilius Engine Integration Concept. Belo Horizonte, 2018. Onera.

[53] L. López de Vega, G. Dufour, and N. Garcia Rosa. Fully Coupled Body Force–Engine Performance Methodology for Boundary Layer Ingestion. Journal of Propulsion and Power, 2021.

[54] J. Bijewitz, A. Seitz, and M. Hornung. Power Plant Pre-Design Exploration for a Turbo-Electric Propulsive Fuselage Concept. In 2018 Joint Propulsion Conference. American Institute of Aeronautics and Astronautics, Reston, 2018.

[55] R. Jansen, M. Celestina, and H. Kim. Electrical Propulsive Fuselage Concept for Transonic Transport Aircraft. Edwards, 2019. NASA Armstrong Flight Research Center.

[56] W. Canders, J. Hoffmann, and M. Henke. Cooling Technologies for High Power Density Electrical Machines for Aviation Applications. Energies, 2019.

[57] M. Sürer and H. Arat. State of Art of Hydrogen Usage as a Fuel on Aviation. European Mechanical Science, 2018.

[58] V. Sethuraman and J. Weidner. Analysis of Sulfur Poisoning on a PEM Fuel Cell Electrode. Electrochimica Acta, 2010.

[59] J. Kallo, M. Renouard-Vallet, G. Saballus, J. Schmithals, J. Schirmer, and K. Friedrich. Fuel Cell System Development and Testing for Aircraft Applications. Essen, 2010. Forschungszentrum Jülich GmbH.

[60] D. Howe. Aircraft Conceptual Design Synthesis. Professional Engineering Pub, London, 2000.

[61] E. Torenbeek. Synthesis of Subsonic Airplane Design. Delft University Press, Delft, 1982.

[62] A. Kundu, M. Price, and D. Riordan. Conceptual Aircraft Design: An Industrial Approach. John Wiley & Sons, Hoboken, 2019.

[63] F. White. Fluid Mechanics. McGraw-Hill Education, NY, 2017.

[64] D. Spalding. A Single Formula for the "Law of the Wall". Journal of Applied Mechanics, 1961.

[65] N. Beck, T. Landa, A. Seitz, L. Boermans, Y. Liu, and R. Radespiel. Drag Reduction by Laminar Flow Control. Energies, 2018.

[66] T. Streit, S. Wedler, and M. Kruse. DLR Natural and Hybrid Transonic Laminar Wing Design Incorporating New Methodologies. Braunschweig, 2014. Cambridge University Press.

[67] B. Woods and M. Friswell. Multi-objective geometry optimization of the Fish Bone Active Camber morphing airfoil. Journal of Intelligent Material Systems and Structures, 2016.

[68] H. Steiner, A. Seitz, Wieczorek, K. Plötner, A. Isikveren, and M. Hornung. Multi-Disciplinary Design and Feasibility Study of Distributed Propulsion Systems. Brisbane, 2012. ICAS.

[69] D. Scholz. High Lift Systems and Maximum Lift Coefficients, 2015.

[70] Bundesregierung. Verordnung zur Umsetzung des Erneuerbare-Energien-Gesetzes 2021 und zur Änderung weiterer energierechtlicher Vorschriften, January 2022.

[71] BDEW Bundesverband der Energie- und Wasserwirtschaft e.V. BDEW Strompreisanalyse Januar 2021. Technical report, Berlin, 2021.

[72] Deutscher Bundestag. Stromsteuergesetz (StromStG), 1999.

[73] Bundestag. Fragen zur Entwicklung der Netzentgelte im Stromsektor. Technical report, 2020.

[74] Deutsche Energie-Agentur GmbH (dena). Power to X: Technologien. Technical report, Berlin, 2018.

[75] MWIDE.NRW. Entwicklung der Strompreise für private und industrielle Verbraucher, mit und ohne staatliche Belastungen. Technical report, 2018.

[76] U. Cardella, H. Decker, and L. Klein. Economically Viable Large-Scale Hydrogen Liquefaction. IOP Conference Series: Materials Science and Engineering, 2017.

[77] R. Pinsky, P. Sabharwall, J. Hartvigsen, and J. O'Brien. Comparative Review of Hydrogen Production Technologies for Nuclear Hybrid Energy Systems. Progress in Nuclear Energy, 2020.

[78] T. Smolinka and et al. Industrialisierung der Wasserelektrolyse in Deutschland: Chancen und Herausforderungen für nachhaltigen Wasserstoff für Verkehr, Strom und Wärme. Technical report, Bundesministerium für Verkehr und digitale Infrastruktur (BMVI), Berlin, 2018.

[79] K. Görner and D. Lindenberger. Technologiecharakterisierungen in Form von Steckbriefen. Technical report, Virtuelles Institut „Strom zu Gas und Wärme", Berlin, 2015.

[80] G. Müller-Syring, M. Henel, W. Köppel, H. Mlaker, M. Sterner, and T. Höcher. Entwicklung von modularen Konzepten zur Erzeugung, Speicherung und Einspeisung von Wasserstoff und Methan ins Erdgasnetz. Technical report, Deutscher Verein des Gas- und Wasserfaches e.V. (DVGW e.V.), 2013.

[81] C. Noack and et al. Studie über die Planung einer Demonstrationsanlage zur Wasserstoff-Kraftstoffgewinnung durch Elektrolyse mit Zwischenspeicherung in Salzkavernen unter Druck. Technical report, Deutsches Zentrum für Luft- und Raumfahrt, Stuttgart, 2015.

[82] C. Kwasi-Effah, A. Obanor, and F. Aisien. A Review on Electrolytic Method of Hydrogen Production from Water. American Journal of Renewable and Sustainable Energy, 2015.

[83] M. Roeb and et al. Wasserstoff als ein Fundament der Energiewende. Teil 1: Technologien und Perspektiven für eine nachhaltige und ökonomische Wasserstoffversorgung. Technical report, German Aerospace Center, Bonn, 2020.

[84] A. Regett and C. Pellinger. Power2Gas – Hype oder Schlüssel zur Energiewende? Energiewirtschaftliche Tagesfragen, 2014.

[85] J. Aghaei and M. Alizadeh. Demand Response in Smart Electricity Grids Equipped with Renewable Energy Sources: A Review. Renewable and Sustainable Energy Reviews, 2013.

[86] M. Klell, H. Eichlseder, and A. Trattner. Wasserstoff in der Fahrzeugtechnik: Erzeugung, Speicherung, Anwendung. Springer Vieweg, Wiesbaden, 2018.

[87] B. Pitschak, J. Mergel, and M. Mueller. Elektrolyse-Verfahren. In B. Pitschak and Jochen Lehmann, editors, Wasserstoff und Brennstoffzelle. Springer Berlin Heidelberg, Berlin, Heidelberg, 2017.

[88] HOMER Energy. Annualized Cost, 2021.

[89] J. Incer, J. Mörsdorf, T. Morosuk, and G. Tsatsaroni. Hydrogen Energy Storage – Exergy-Based Analysis of the Charging Process. Poland, 2020. Institute for Energy Engineering, Technische Universität Berlin.

[90] E. Taibi, H. Blanco, R. Miranda, and M. Carmo. Green Hydrogen Cost Reduction. Scaling Up Electrolysers to Meet the 1.5°C Climate Goal. Technical report, International Renewable Energy Agency (IRENA), online, 2020.

[91] European Commission. Horizon 2020 Framework Programme: Develop and Demonstrate a 100 MW Electrolyser Upscaling the Link between Renewables and Industrial Applications, 2020.

[92] L. Bertuccioli, A. Chan, D. Hart, F. Lehner, B. Madden, and E. Standen. Study on Development of Water Electrolysis in the EU. Technical report, E4tech Sàrl with Element Energy Ltd, Lausanne, 2014.

[93] E. Connelly, M. Penev, A. Elgowainy, and C. Hunter. Current Status of Hydrogen Liquefaction Costs. DOE Hydrogen and Fuel Cells Program Record 19001, US Department of Energy, 2019.

[94] D. Krieg. Konzept und Kosten eines Pipelinesystems zur Versorgung des deutschen Straßenverkehrs mit Wasserstoff. Forschungszentrum Jülich, Jülich, 2012.

[95] United States Driving Research and Innovation for Vehicle efficiency and Energy sustainability (U.S. DRIVE). Hydrogen Delivery Technical Team Roadmap. Roadmap, Washington, 2013.

[96] C. Yang and J. Ogden. Determining the Lowest-Cost Hydrogen Delivery Mode. International Journal of Hydrogen Energy, 2007.

[97] J. Fischedick and et al. Shell Hydrogen Study. Energy of the Future? Sustainable Mobility through Fuel Cells and H2. Technical report, Shell Deutschland Oil GmbH, Hamburg, 2017.

[98] M. Oostdam. Techno-Economic Assessment of a Hydrogen Fuel-Cell Tractor Semi-Trailer. Exploratory Research into the Feasibility. PhD thesis, Delft University of Technology, Delft, 2019.

[99] C. Walker. All-Causes Delay and Cancellations to Air Transport in Europe. Annual Report for 2019. Technical report, Eurocontrol, -, 2020.

[100] G. Petitpas. Boil-Off Losses Along LH2 Pathway. Technical report, Lawrence Livermore National Laboratory, Livermore, 2018.

[101] U. Schmidtchen and E. Behrend. Hydrogen Aircraft and Airport Safety. Renewable and Sustainable Energy Reviews, 1997.

[102] Airbus S.A.S. A319. Aircraft Characteristics. Airport and Maintenance Planning, 2020.

[103] ICAO. Annex 14 to the Convention on International Civil Aviation - Volume I, Aerodrome Design and Operations. Technical report, ICAO, Washington, 2020.

[104] Fuel Cells and Hydrogen 2 Joint Undertaking. Hydrogen-Powered Aviation: A Fact Based Study of Hydrogen Technology, Economics, and Climate Impact by 2050. Publications Office, LU, 2020.

[105] European Commission. Commission Regulation (EC) No 8/2008 - Common Technical Requirements and Administrative Procedures Applicable to Commercial Transportation by Aeroplane, 2007.

[106] F. Svensson, A. Hasselrot, and J. Moldanova. Reduced Environmental Impact by Lowered Cruise Altitude for Liquid Hydrogen-Fuelled Aircraft. Aerospace Science and Technology, 2004.

[107] J. Green. Air Travel – Greener by Design Mitigating the Environmental Impact of Aviation: Opportunities and Priorities. The Aeronautical Journal (1968), 2005.

[108] H. Mannstein and U. Schumann. Aircraft Induced Contrail Cirrus Over Europe. Meteorologische Zeitschrift, 2005.

[109] L. Ström. First Simulations of Cryoplane Contrails. Journal of Geophysical Research, 2002.

[110] MIT Global Airline Industry Program. Airline Data Project. Aircraft and Related, 2020.

[111] K. Franz. CeRAS Direct Operating Cost (DOC) Model, 2014.

[112] D. Rutherford, B. Zheng, X. Graver, and N. Pavlenko. Potential Tankering Under an EU Sustainable Aviation Fuels Mandate. International Council on Clean Transportation, 2021.

[113] J. O'Malley, N. Pavlenko, and S. Searle. Estimating Sustainable Aviation Fuel Feedstock Availability to Meet Growing European Union Demand, 2021.

[114] Argus Media Group. EU ETS Price €32-65/t Under 2030 Scenarios, 2020.

[115] Airbus Media Relations. Airbus Aircraft 2018 Average List Prices, 2019.

[116] European Commission. The European Green Deal. Brüssel, 2019. European Commission.